Effect of Domain Boundaries on the Raman Spectra of Mechanically Strained Graphene

Mark A. Bissett,[†] Wataru Izumida,[‡] Riichiro Saito,[‡] and Hiroki Ago[†,*]

[†]Institute for Materials Chemistry and Engineering, Kyushu University, Fukuoka 816-8580, Japan and [‡]Department of Physics, Tohoku University, Sendai 980-8578, Japan

ABSTRACT

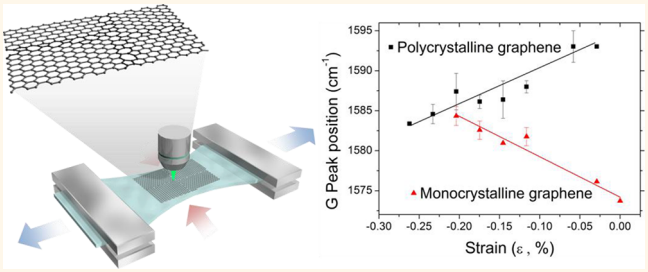

We investigate the effect of mechanical strain on graphene synthesized by chemical vapor deposition (CVD) transferred onto flexible polymer substrates by observing the change in the Raman spectrum and then compare this to the behavior of exfoliated graphene. Previous studies into the effect of strain on graphene have focused on mechanically exfoliated graphene, which consists of large single domains. However, for wide scale applications CVD produced films are more applicable, and these differ in morphology, instead consisting of a patchwork of smaller domains separated by domain boundaries. We find that under strain the Raman spectra of CVD graphene transferred onto a silicone elastomer exhibits unusual behavior, with the G and 2D band frequencies decreasing and increasing respectively with applied strain. This unusual Raman behavior is attributed to the presence of domain boundaries in polycrystalline graphene causing unexpected shifts in the electronic structure. This was confirmed by the lack of such behavior in mechanically exfoliated large domain graphene and also in large single-crystal graphene domains grown by CVD. Theoretical calculation of G band for a given large shear strain may explain the unexpected shifts while the shift of the Dirac points from the *K* point explain the conventional behavior of a 2D band under the strain.

KEYWORDS: flexible · graphene · Raman · strain · domain boundary · CVD · PDMS

Graphene has been the focus of a wide variety of research regarding its unique materials properties. These unique properties include a high degree of mechanical strength as well as elasticity,[1] excellent charge carrier mobility,[2] optical transparency,[3] and chemical stability.[4] These properties make graphene an attractive material for wide-scale integration into electronic devices. The ability to fully understand the properties of this unique material under a wide range of conditions is paramount to any future applications. Of particular interest to the field of flexible electronics is the effect of stress and strain on the lattice of graphene and the resulting change in the electronic structure, particularly when in contact with a flexible substrate. Altering of the electronic structure could lead to strain engineering to produce a specific electronic structure or possibly introduce a band gap.[5−8] The interfacial strain transfer between graphene and an underlying polymer is also of interest for the creation of high strength composite matrices.[9−11]

There have been several previous publications that investigate the effect of strain on graphene. These have included substrate induced strain due to the lattice mismatch between graphene and the underlying substrate,[12,13] as well as the effect of applied mechanical strain on the resistivity and conductivity of stretchable transparent electrodes,[14−16] but most research has focused on the effect of strain on the Raman spectrum of graphene.[10,11,17−32] This is of particular importance as it gives an accurate indication of the electronic structure and phonon transport properties that differ as the graphene crystal structure is altered. Previous studies have included both uniaxial[18−20,26,27] and to a lesser extent biaxial[21,24,32] strain and the resultant effects on the Raman spectrum, most notably a shift in the G and 2D (or G′) band peak frequency. This shift in Raman peak frequency is caused by the distortion of the graphene lattice, which in turn alters the vibrational Raman frequency of the phonons within the lattice. Typically, compression of the graphene lattice leads to a phonon hardening (frequency upshift), while tension leads

* Address correspondence to ago@cm.kyushu-u.ac.jp.

Received for review August 31, 2012 and accepted October 6, 2012.

Published online October 07, 2012
10.1021/nn304032f

to phonon softening (frequency downshift). The rate of this change in peak position with strain is an intrinsic property of the material and is defined by its Grüneisen parameters, which describe how changing the volume of a crystal lattice affects its vibrational properties.[33]

Previous literature reports on the Raman behavior of graphene under strain deal mainly with mechanically exfoliated graphene that is transferred onto a polymer substrate. These polymer substrates include polymethyl methacrylate (PMMA),[9,11,22,25,27,28,31] polyethylene terephthalate (PET),[18,19,26,33] and polydimethylsiloxane (PDMS).[10,14−16,20,29] Each polymer has different properties that alter the amount of strain that can be exerted onto the graphene. Exfoliated graphene transferred onto a flexible polymer provides a large (10−100 μm sized) single domain area to analyze; however, for industrial scale applications when large area (>cm) graphene films are required, the behavior of chemical vapor deposition (CVD) synthesized graphene will be of most interest. The crystal domain structure differs for exfoliated graphene and CVD-grown graphene.[34−40] Mechanically exfoliated graphene mostly exists as large single domain flakes, often with a differing number of layers, whereas CVD-grown graphene generally exhibits a continuous single-layer film consisting of a large number of smaller domains, when synthesized on a polycrystalline foil.[36] There have been very few investigations into the properties of CVD-grown graphene under applied strain, with recent works using infrared spectroscopy to investigate the transmission properties of strained CVD graphene[41] and biaxial strain applied to large-domain suspended graphene.[42] The domain size of polycrystalline graphene synthesized on copper foil is an average of 1 μm with a range of domain sizes ranging from several hundred nanometers to 1−2 μm as determined by low energy electron microscopy (LEEM),[40] and the spot size of the confocal Raman laser used is also approximately 1 μm. Thus, when performing Raman spectroscopy of polycrystalline graphene there is a high probability of observing domain boundaries. The presence of these numerous domain boundaries is detrimental to the mobility of charge carriers within the graphene due to phonon scattering, with the carrier mobility in CVD-grown single-layer graphene on the order of 1000−4000 $cm^2/(V\ s)$ compared to exfoliated graphene with mobility's of up to 10 000 $cm^2/(V\ s)$ when measured on SiO_2/Si substrates.[43−45] Domain boundaries are believed to alter the electronic band structure possibly introducing a band gap,[38,46] as well as altering the mechanical properties of graphene.[47−49] The cause for this detrimental behavior has been investigated, and it has been shown that these domain boundaries will cause an increase in the phonon scattering due to grain orientation mismatch.[43,50]

In this work we compare the strain behavior of polycrystalline CVD-grown graphene to that of exfoliated graphene, by confocal Raman spectroscopy. From previous investigations we expect the strain behavior at the domain boundaries to be different from the inside of the domains.[47,49,51] These theoretical models of polycrystalline graphene show that strain is homogenously distributed inside graphene grains while domain boundaries experience increased strain.[47,49] The second-order Raman process responsible for the 2D band is caused by the scattering of two iTO phonons near the K point and is independent of defects,[52] instead it is affected only by strain and provides information about the conditions inside of the domains. On the other hand, the D band originates from a single iTO phonon combined with phonon scattering from a defect, such as those along domain boundaries, and it offers information about the strain at the boundary. The G band originates from a first-order single phonon Raman process, thus it is affected by strain both within the domain and at the boundary. This provides information on the change in the force constant and distribution of strain. Therefore, by comparing different Raman peaks under strain, we investigate the effect on graphene domains which are comparable to the laser spot size. It is found that the domain boundaries present in CVD graphene cause an anomalous behavior in the shift of Raman peak positions together with peak broadening, and several possible causes for these results are discussed in combination with theoretical analysis. Gaining an understanding as to the reasons for this behavior as well as identifying the cause are essential to any applications, such as flexible electronics, involving CVD graphene that undergoes stress. Large single domain graphene grown by CVD was also investigated and compared. The comparison between two different polymer substrates are also investigated, the relatively rigid PMMA, and the highly flexible PDMS exhibit differing behavior due to interfacial strain transfer to the graphene.

RESULTS AND DISCUSSION

Synthesis of Flexible Graphene Substrates. To first confirm that graphene had been successfully synthesized and transferred onto the desired polymer substrate, Raman spectra were taken at the various stages (see Supporting Information, Figure SI-1). The spectrum of CVD-grown graphene transferred onto SiO_2 shows the characteristic Raman peaks at 2675 cm^{-1} (2D or G′ band) and 1590 cm^{-1} (G band) and a low intensity peak at 1340 cm^{-1} (D band). The relative intensity and width of these peaks indicate that the graphene is single-layer and of high quality.[53,54] After transfer of the graphene onto a PDMS substrate, the characteristic Raman peaks could be detected indicating successful transfer of graphene, this was also possible for the graphene on the PMMA substrate. Once graphene has been successfully attached to a flexible supporting

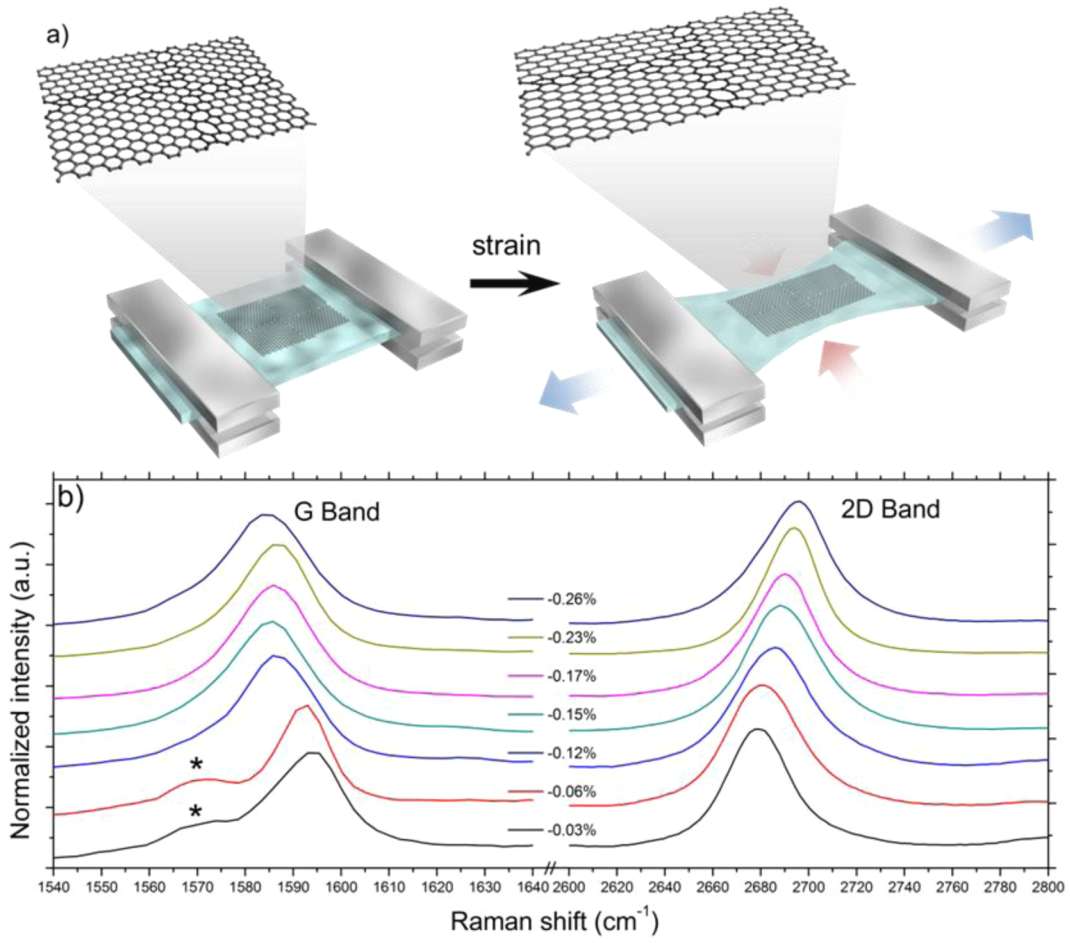

Figure 1. (a) Schematic of graphene lattice on PDMS substrate undergoing strain. (b) Raman spectra of graphene on PDMS for increasing applied tension. Note the opposite shift in G and 2D band frequency. Asterisks denote a peak from PDMS substrate.

substrate, the effect of strain on the Raman spectrum can be observed. Figure 1 illustrates the effect of strain on the lattice structure of CVD-grown graphene on a PDMS substrate and the resultant Raman spectra. After stress is applied the lattice is distorted and the interatomic distance altered, shifting the phonon frequency. Figure 1b shows the Raman spectra with increasing strain. There is a clear shift in the frequency of both the G and 2D bands, with the G band showing a downshift while the 2D band upshifts. This is unexpected behavior as previous literature using exfoliated graphene observed that both the G and 2D bands downshift when the sample is stretched.[24,33]

Since we use a PDMS elastomer substrate with a high Poisson's ratio (0.5), we expect longitudinal elongation and transverse contraction of the graphene sample. This asymmetrical strain causes a change in the graphene hexagonal lattice symmetry. It has been noted previously that applied tensile strain leads to a uniformly compressed graphene unit cell.[5] This result indicates that the graphene sheet undergoes significant lateral compression with uniaxial tension, which is a unique feature of PDMS rubber. This same compression effect induced by applied tension has been observed previously in the literature of graphene–PDMS composite materials.[10] In this previous work, the authors note that at high applied tension the Raman peak shift became compressive, and they attribute this change to the high mobility of PDMS chains at room temperature leading to lateral compression of the graphene.[10] This is related to the Poisson's ratio of the PDMS which causes lateral compression when uniaxial tension is applied. Thus, our observed upshift of the 2D band is consistent with previous results showing the compression of graphene on PDMS.

We also observe a significant increase in the peak width of G and 2D bands, indicative of applied strain causing a splitting of the phonon bands or/and inhomogeneous distribution of strain in the sample which will be discussed in further detail in what follows. To gain a better understanding of the peak shift behavior we increase the strain incrementally on the substrate and simultaneously measure the shift in Raman peak frequency and plot this against percentage strain. We then compare the behavior of both exfoliated and CVD-grown graphene.

Unlike many previous studies in which the graphene is bent to induce strain, in this work the tension

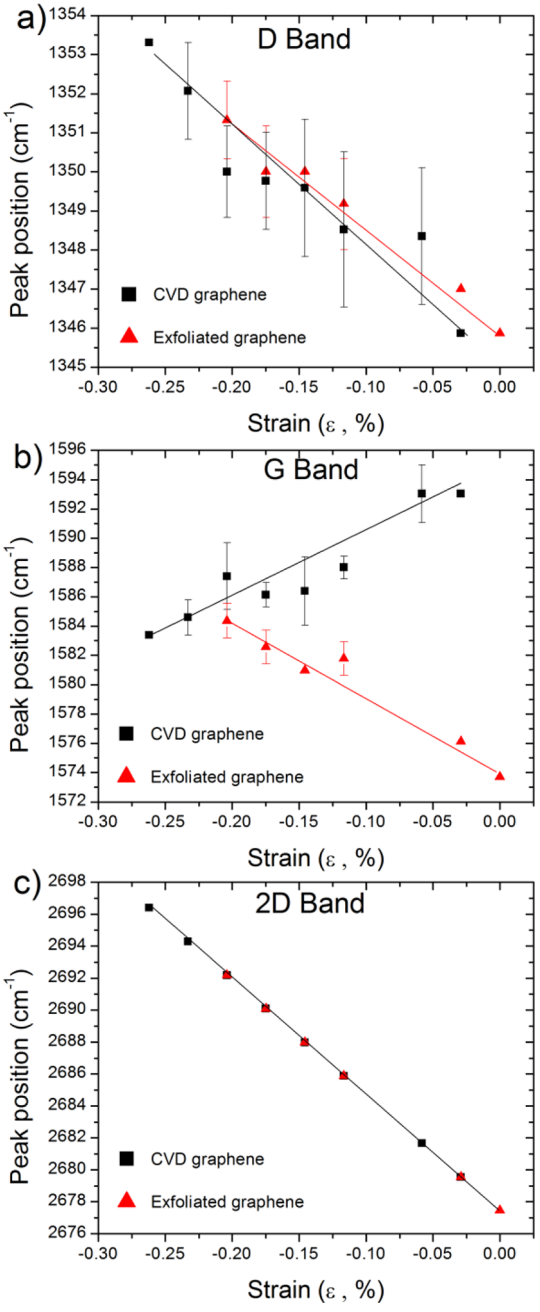

Figure 2. Plots of Raman peak shift with applied strain for CVD-grown and exfoliated graphene on PDMS substrates. Error bars are one standard deviation: (a) D band, (b) G band, and (c) 2D band.

is applied longitudinally, along the basal plane. Graphene is significantly more rigid along this basal direction and the maximum strain that can be achieved is thus lower, in this work values of around 0.2−0.3% appear to be the maximum that can be achieved, as seen in Figure 2. This may be related partly to increased rigidity of graphene, but also inefficient interfacial strain transfer between the polymers and the graphene at higher strain values.[9,10,31] Owing to the discrepancy in the applied strain to the polymer substrate and the strain exerted on the graphene, the Raman peak shift was used to create a calibration curve to more accurately reflect the "real" strain being exerted on the graphene. It has been shown previously that inefficient strain transfer between the polymer and graphene can lead to lower values of strain being exerted on the graphene than by simply calculating the strain being exerted on the polymer substrate alone. This method of creating a calibration curve based on peak shift to find the "real" strain has also been demonstrated in the literature.[8,24] By using the formula given by *Mohiuddin et al.* we can calculate the exerted strain based on Raman peak position shift, as shown in eq 1.[33] Where γ is the Grüneisen parameter, $\Delta\omega$ is the Raman frequency shift with applied strain, ω_0 is the Raman frequency with no applied strain, ν is the Poisson's ratio of the substrate material, and ε is the % strain applied to the sample.

$$\gamma = \frac{\Delta\omega}{2\omega_0(1-\nu)\varepsilon} \quad (1)$$

Owing to the excellent strain sensitivity and high signal intensity of a 2D peak for single-layer graphene, it is an ideal peak to calibrate the strain. Also the origin of the 2D Raman peak comes from the second-order process involving two iTO phonons without the need for a defect. Thus, all strain values shown in this work are calibrated to the shift of the 2D peak. There is a certain degree of disagreement in the literature on the exact value of the Grüneisen parameter for the 2D band, with differing values being reported due to different supporting substrates or calculation methods. In this work we take the Grüneisen parameter for the 2D peak calculated from first principles by *Mohiuddin et al.* to be 2.7.[33] Should a more appropriate Grüneisen parameter be determined for polycrystalline graphene that takes into account the effect of domain boundaries the strain calibration can be altered, without affecting the trends discussed in this work. By calibrating the shift in Raman peak position the actual strain being exerted onto the graphene can be known more accurately, removing the factor of inefficient strain transfer from the supporting substrate, this then allows us to more accurately plot the shift of the other Raman peaks. This gives a slope of -72 cm^{-1}/% for the plot of 2D *versus* % strain; this value of slope is dependent only on the Grüneisen parameter used to calculate strain.

Many previous reports into strained graphene observed a splitting of the G peak into two distinct peaks, named the G^+ and G^- with analogy to carbon nanotubes; however, this distinct splitting was not observed in this work. Instead a peak broadening was observed, as the full width at half-maximum (fwhm) of the G peak increased linearly with applied strain (see Supporting Information, Figure SI-2). This broadening, instead of discrete splitting, can be attributed to the lower strain exerted onto the graphene; typically two distinct peaks are only able to be resolved above 0.3−0.4% strain.[20,25,28,33,55] Thus, for the results shown here the

TABLE 1. Slope of Raman Peak Shift for Exfoliated and CVD Graphene

Raman peak	exfoliated graphene ($\partial\omega/\partial\varepsilon$) (cm^{-1})	CVD graphene ($\partial\omega/\partial\varepsilon$) (cm^{-1})
D band	−25.1	−25.0
G band	−49.3	41.1
2D (G′) band	−72.3	−72.3

peak shift here is given for a single G peak. Theoretical calculations of this peak broadening will be discussed in more detail later.

Comparison of Exfoliated and CVD-Grown Graphene. As previously discussed, all previous studies in the Raman behavior of graphene when undergoing strain have been focused on the use of large domain exfoliated graphene. When we compare the strain behavior of exfoliated graphene to that of CVD-grown graphene we observe a distinctly different behavior of the slope of the peak shift with strain, which can be seen in Figure 2b. When we apply strain to CVD graphene and plot the peak shifts we observe that the $\partial\omega/\partial\varepsilon$ values for the 2D band overlay one another as this is the calibration curve, the D band shift is also very close for each, however, the for G bands have opposite sign slopes. The magnitude of $\partial\omega/\partial\varepsilon$ for each sample is similar, and these are listed in Table 1.

The close match between the D band data for each sample is to be expected as the frequency is directly related to that of the 2D band, which is an overtone of the D band. The opposite signs of the G band observed for CVD graphene indicate that as the graphene undergoes phonon hardening, given by the increase in 2D band frequency, simultaneously the G band is decreasing in frequency or undergoing phonon softening. When strain is applied to single domain graphene, phonon hardening and softening occur as a result of the lattice distortion; however, when polycrystalline material is strained, several other mechanisms can occur which include not only tension and compression but also domain rotation and slippage and these may be responsible for such a Raman shift. To ensure that applied strain was not generating defects in the graphene lattice, such as tears or wrinkles, the I_D/I_G ratio was plotted with increasing strain (see Supporting Information, Figure SI-3). It was observed that the I_D/I_G ratio stayed approximately constant with increasing stress, indicating that defects were not being introduced into the graphene lattice by applying strain. Note that excessive strain induced the breakage of the graphene film as well as the polymer substrate so that the applied strain was set within this limit.

To support the hypothesis that it is the presence of domain boundaries that causes the unusual Raman behavior seen in polycrystalline graphene, large single-domain graphene was synthesized by CVD using sputtered copper on a c-plane sapphire substrate. This has been shown previously to produce large hexagon-shaped domains, due to the optimized growth conditions (low CH_4 concentration and high temperature).[56,57] Figure 3a illustrates the resulting hexagonally shaped graphene domains after transfer onto PDMS, and the subsequent distortion of the hexagonal shape with applied strain. The percentage of observed strain, calculated from the change in size of the hexagon, is seen to be much higher than that calculated from the graphene peak shift. This is in agreement that not all strain is transferred from the substrate into the graphene lattice due partially to increased rigidity of the graphene and also poor interfacial strain transfer. Figure 3b shows the resulting Raman spectra from the large domain graphene with increasing strain, while Figure 3c,d shows plots of the peak shift with applied strain. The graphene produced by this method consists of a large single domain, in this case the domain size is approximately 100 μm, as opposed to the 1 μm domain size produced on polycrystalline foil.[40] Figure 3c,d clearly shows that both the G and 2D band shift with the same slope, matching the exfoliated graphene. This strongly supports that it is the strain present at domain boundaries that causes the opposite trend in the G and 2D band shift with applied strain (see Figure 2). However, some damage to the graphene is caused by the transfer process; although these point defects do not appear have the same effect as a domain boundary.

This unexpected behavior appears to be specific to small domain CVD-grown graphene and not a substrate induced effect. To verify this, CVD graphene was investigated by Raman on both PDMS and PMMA as was exfoliated graphene, and in each case exfoliated graphene followed the expected trend from literature, independent of the substrate material, while CVD graphene exhibited the opposite slope for the G and 2D bands (see Supporting Information, Figure SI-4). When CVD and exfoliated graphene is compared, the key difference, as has been discussed previously, is that exfoliated graphene exists as a large single domain while CVD graphene is created from small individual nucleation sites that create a large polycrystalline film. These domain boundaries are the key difference between the types of graphene being investigated in this work. Previously, it has been shown using theoretical calculations that the presence of domain boundaries in CVD graphene can alter their behavior in nanoresonators, due to the breaking of symmetry and introduction of pentagon−heptagon (5−7) pairs along the boundaries.[50] Atomistic simulations of polycrystalline graphene undergoing strain have also shown that domain boundaries, particularly 5−7 pairs, undergo increased strain when compared to the rest of the domain structure.[49] The presence of defects in carbon nanotubes under strain has also been previously investigated on an atomic scale, and it was found that defective regions undergo

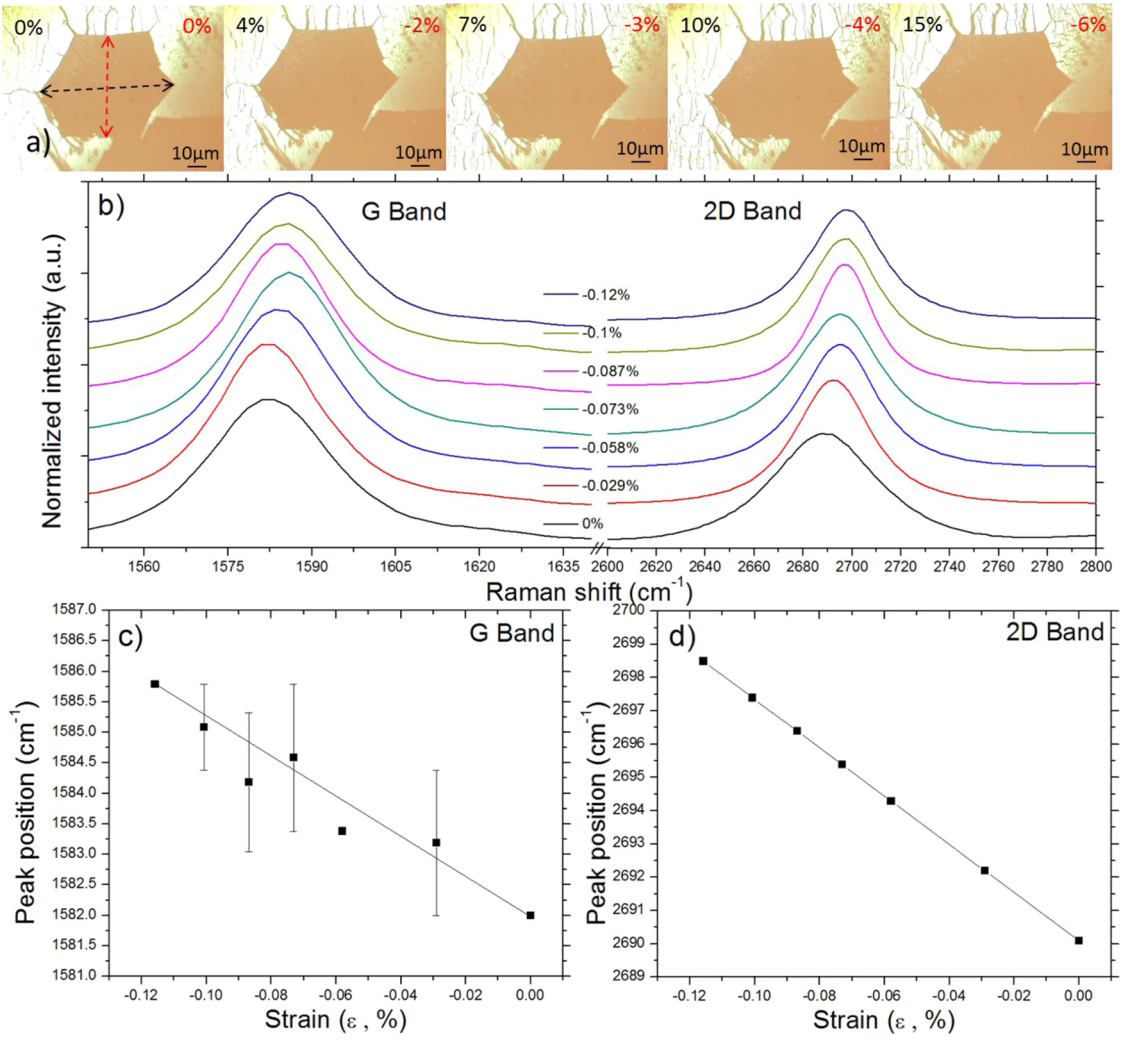

Figure 3. (a) Optical microscope images of large hexagonal CVD-grown graphene domains after transfer onto PDMS substrate with increasing applied strain. Percentages are elongation and compression measured visibly by substrate distortion. (Note the discrepancy between applied strain measured optically and measured strain given by graphene peak shift.) (b) Raman spectra of large domain graphene with increasing strain showing shift in peak position. (c,d) Plots of Raman peak shift with applied strain for large domain graphene. Error bars are one standard deviation.

significantly increased strain when compared to defect-free tubes.[58] It was also noted that the curvature of the tube had little influence, and thus we can apply these conclusions to graphene. A wide variety of defects can be present along grain boundaries; including 5−7 dislocations, Thrower−Stone−Wales defects, double pentagon−octagon (5−8−5), and various other clusters.[59,60] The presence of these defects has been shown to cause a blue shift of the Raman G band.[61] Extended line defects, in the form of a domain boundary, can act like an independent nanowire imbedded within the larger graphene lattice affecting charge transport properties and Raman spectra.[62,63] These previous studies support that the presence of domain boundaries can indeed significantly affect the electronic structure of the graphene.

Theoretical Models. To explain the experimental results, theoretical calculations were performed to predict Raman behavior of graphene while under strain. The details of calculations are described in the Supporting Information. In the present tight-binding calculation method for Raman spectra, effects of domain boundaries that may have 5−7 ring pairs and others are not taken into account, thus the description is limited to the hexagonal lattice. When strain is applied to the graphene lattice there are changes to the hopping integral between the neighboring π-orbitals of the carbon atom which alter the electronic energy bands in the deformed Brillouin zone. Then, the wave vector of the 2D band which satisfies the double resonance Raman theory gives the positive and negative shifts of the 2D peak as a function of the strain in the longitudinal and transverse directions (ε_l and ε_t, see eqs 3 and 4 in the Supporting Information). By using the linear energy dispersion of the electronic band near the *K* point, we estimate the shift of the 2D band (see eq 10 in the Supporting Information). These shifts depend on the orientation of the applied strain, both longitudinal and transverse. The distance between one Dirac point and its three

nearest neighbor atoms in the graphene lattice can be altered under applied strain, and this causes the splitting of the 2D band into three separate peaks.[8,27] For an applied strain of ~0.3% we calculate that the 2D peak splitting should be ~6 cm^{-1}, this is consistent with our experimental observation shown in Supporting Information, Figure SI-2.

Owing to the complexity and disorder present along domain boundaries it is difficult to accurately predict phonon behavior using theoretical calculations. There are several possible explanations to understand the cause of the unusual G band behavior of polycrystalline graphene. As well as the contribution of domain boundaries and the effect they have on phonon scattering while undergoing strain there are also contributions from substrate interactions. The interaction with a flexible substrate through hydrostatic deformation and shear strain can cause a change in the force constant, affecting strain behavior.[64] By calculating using the same strain in both the longitudinal and transverse directions, we estimate the shift of G band using the previous works discussed by Reich *et al.*[64] by taking into account a linear correction of the strain to the force constant. The G band splitting into G^+ and G^- bands is given by

$$\frac{\delta\omega_{G\pm}}{\omega_{G0}} = -\lambda\varepsilon_h \pm \frac{1}{2}\beta\varepsilon_s \qquad (2)$$

where $\delta\omega_{G\pm} = \omega_{G\pm} - \omega_{G0}$, ω_{G+}, and ω_{G-} are the phonon frequencies of G^+ and G^- bands, respectively, with strain, and ω_{G0} is the phonon frequency without strain. $\varepsilon_h = \varepsilon_l + \varepsilon_t$ is the hydrostatic component of the strain, and $\varepsilon_s = \varepsilon_l - \varepsilon_t$ is the shear component of the strain, where ε_l (ε_t) is the longitudinal (transversal) strain. The coefficient λ is the Grüneisen parameter, which describes the frequency shift under a hydrostatic deformation, and the coefficient β describes the frequency shift for a shear strain. The coefficients are estimated as $\lambda = 1.99$ and $\beta = 0.99$ for the G band of graphene under a uniaxial strain.[33]

One expects a small hydrostatic deformation for a graphene transferred onto a flexible polymer substrate, because a two-dimensional area would be almost conserved under a strain, which leads a relation $\varepsilon_t \approx -\varepsilon_l$, therefore $\varepsilon_h \approx 0$ and $\varepsilon_s \approx 2\varepsilon_l$. For this case, the G band modification is dominated by the second term in eq 2, and the peak splits into two, one peak with hardening and one peak with softening (see Supporting Information, Figure SI-5 for the calculated result). The shift is estimated to be $\delta\omega_{G\pm} = \pm 5$ cm^{-1} for $\varepsilon = 0.3\%$, this magnitude is comparable to that shown in Figure 2b of the experimental results.

We can show that the opposite slope of the G band occurs if the transverse strain is larger than that expected by the Poisson's ratio. Such a situation may be possible for a flexible substrate in which we expect a large shear strain on the substrate with transfer to graphene. However, if this is the only reason for the G band behviour, this effect should appear for a large single domain graphene, which does not adequetly explain the observed experimental results. We should consider the strain at the domain boundary and phonon frequency as a future subject of study. It should be noted that if we stretch, for example, a seven-member ring, we expect a large transverse strain.[49] Although we need a further theoretical investigation for the phonon frequency for five- and seven-member rings, as the geometical structure at the domain boundary has not been well determined yet.

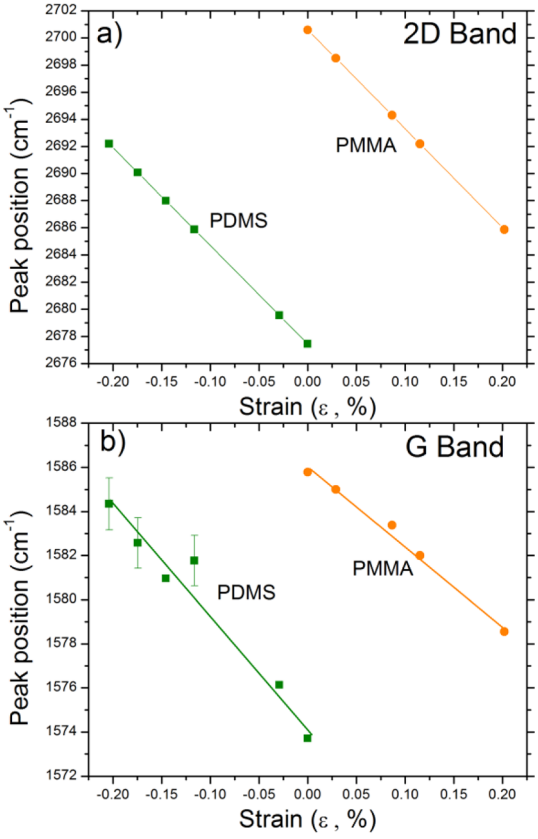

Figure 4. Plots of Raman shift with applied strain for exfoliated graphene on both PDMS and PMMA substrates showing compressive and tensile behavior: (a) 2D band and (b) G band. Error bars are one standard deviation.

Strain Induced by PMMA and PDMS. The interfacial stress transfer between graphene and a polymer substrate can affect the exerted stress experienced by the graphene. Figure 4 shows the calibration curve for the 2D peak along with the measured G peak shifts for exfoliated single-layer graphene on both PMMA and PDMS substrates. The large offset at zero applied strain is mainly caused by substrate induced prestrain due to interactions between the polymer and graphene layer during synthesis/transfer. This prestrain is believed to be caused primarily by the curing of the polymer substrate in contact with the graphene as well as some residual strain due to the crystal lattice offset of the copper foil. There is also slight strain exerted onto the sample during the loading procedure into the experimental strain rig. When strain is applied to the graphene

on a PMMA substrate a decrease in peak frequency occurs with increasing strain, and this is defined as positive strain. This positive strain indicates tension is being applied to the graphene lattice. However, when strain is applied to the graphene on a PDMS substrate an increase in peak frequency is observed, defined as negative strain (see Figure 1). The cause of this compression can be attributed to the mechanical properties of the polymer substrate. In the case of PMMA, the Poisson's ratio is 0.37 while PDMS has a higher value of 0.5, indicating that while the PDMS sample is undergoing tensile strain there is significant compression perpendicular to the direction of applied strain.[14,65] As discussed previously, the use of PDMS causes an asymmetrical strain to be exerted onto the graphene leading to a breaking of symmetry within the graphene crystal lattice.

The magnitude of the slope for the G band frequency shifting with strain ($\partial\omega/\partial\varepsilon$) in Figure 4 is -36 cm^{-1}/% and -49 cm^{-1}/% for PMMA and PDMS, respectively. This value for PMMA matches closely those reported in the literature previously for graphene under tension, with an approximate average literature value of -33 cm^{-1}/%.[25,27,28,30,33,55,66] However, the value of -49 cm^{-1}/% for PDMS is higher than the values typically reported, and this indicates an increased sensitivity to strain when using PDMS as the supporting substrate. This is logical with the previous observation that the graphene is undergoing simultaneous compression and tension due to the materials properties of PDMS, leading to the biaxial stress with applied uniaxial strain. It has also been noted previously that the values of $\partial\omega/\partial\varepsilon$ are nonlinear when moving from compression to tension and this changing slope when in the compressive regime may also explain the discrepancies between the measured values on PMMA and PDMS.[22,25]

CONCLUSIONS

We have shown here that the Raman spectrum of polycrystalline graphene synthesized by CVD behaves distinctly different from large domain exfoliated graphene under applied mechanical strain. The anomalous Raman behavior was found to be specific to polycrystalline CVD graphene and was independent of the flexible polymer substrate used to transfer the strain. This strain caused an unusual shift in the G band of the Raman spectra, and has been attributed to the presence of domain boundaries, presumably 5−7 atomic pairs, formed in the CVD growth procedure. Theoretical modeling suggests that large shear strain present due to these domain boundaries may be responsible for the unexpected Raman shift observed. However, due to the complexity and wide variety of defects present at domain boundaries it is difficult to accurately model the electronic conditions while undergoing strain and further work is still needed to fully explain both the geometry and the electronic structure effects of domain boundaries in polycrystalline graphene. It is essential to understand these effects on the electronic structure that such grain boundaries have when wide-scale application of CVD graphene, such as flexible electronic displays, is realized.

METHODS

Flexible Graphene Substrate Production. Single-layer graphene was prepared by two methods: First by mechanical exfoliation of graphite (highly oriented pyrolytic graphite, STM-1 grade, Advanced Ceramics Corporation, USA) by the adhesive tape method as has been well documented previously,[67] and second, by an atmospheric CVD process on copper foil that has also been reported previously.[40] Briefly, copper foil (Alfa Aesar, 25 μm thick, 99.8% purity) was placed into a tube furnace with a 26 mm ϕ quartz tube and annealed under a hydrogen (20 sccm) and argon (800 sccm) atmosphere at 1000 °C for 60 min, followed by graphene growth using methane (0.5 sccm) as the carbon source for 10 min. This method has been shown to produce large area films of single-layer pristine graphene, the quality of which was verified using Raman spectroscopy prior to any further experiments (see Supporting Information, Figure SI-1). To produce the substrates for strain analysis exfoliated graphene was transferred onto a precured PDMS (Sylgard 184 Elastomer Kit, Dow Corning, USA) substrate that was then strained using a custom uniaxial strain rig (for further details see Supporting Information, Figure SI-9). For exfoliated graphene on PMMA a similar method was used, whereby graphite was exfoliated and then transferred onto a Si/SiO_2 wafer before liquid PMMA (4% in toluene, MW = 960 000) was spin coated on top and cured. After curing the PMMA/exfoliated graphene was peeled off. In the case of CVD-grown graphene, after growth on the copper foil liquid PDMS or PMMA was spin coated and cured before removing the copper foil in aqueous 1 M $FeCl_3$, leaving the cured PDMS/PMMA with the attached graphene layer.

Large-Domain Graphene Substrate Production. A copper film (500 nm thickness) was deposited onto a c-plane sapphire substrate (Kyocera, Japan) with a power of 300 W in an argon atmosphere (0.6 Pa) by radio frequency (RF) magnetron sputtering (Shibaura Mechatoronics Corp., CFS-4ES, Japan). For the growth of graphene, the substrate was heated in a quartz tube and annealed for 40 min under ambient pressure with a gas flow of H_2/Ar (concentration of H_2 is 2.5%) at 1000 °C then increased to 1075 °C over 20 min. Graphene growth is then undertaken by introducing CH_4 and Ar gas (CH_4 = 10 ppm, H_2 = 2.25%) for 20 min. Finally, the sample was rapidly cooled down to room temperature. For transfer onto flexible substrates, PDMS resin was spin coated onto the graphene and cured before dissolving the copper layer in aqueous 1 M $FeCl_3$ leaving the large domain graphene attached to the PDMS substrate.

Raman Spectroscopy Measurements. Analysis was performed using confocal Raman spectroscopy (Nanofinder 30, Tokyo Instruments, Japan) using a laser excitation wavelength of 532 nm with a power of 5 mW and a 100× objective with a numerical aperture of 0.9 and a standard grating (600g/mm). A high resolution grating (1200g/mm) was also used in an attempt to resolve Raman peak splitting, although similar spectra were obtained.

Conflict of Interest: The authors declare no competing financial interest.

Supporting Information Available: Raman spectra of graphene before and after transfer to flexible substrates, fwhm plots for both CVD and exfoliated graphene on PDMS, Raman I_D/I_G ratio of strained graphene, plots of ($\partial\omega/\partial\varepsilon$) for CVD and

exfoliated graphene on both PDMS and PMMA, detailed description and pictures of experimental strain setup, interfacial strain transfer mapping of graphene on PDMS, and further details regarding the theoretical tight binding calculations. This material is available free of charge *via* the Internet at http://pubs.acs.org.

Acknowledgment. We acknowledge K. Kawahara for assistance in producing the single crystal graphene. This work was supported by the JSPS Funding Program for Next Generation World-Leading Researchers (NEXT Program, GR075). R. Saito and W. Izumida acknowledge MEXT Grant No. 20241023 and Grant No. 22740191, respectively.

REFERENCES AND NOTES

1. Lee, C.; Wei, X.; Kysar, J. W.; Hone, J. Measurement of the Elastic Properties and Intrinsic Strength of Monolayer Graphene. *Science* **2008**, *321*, 385–388.
2. Geim, A. K. Graphene: Status and Prospects. *Science* **2009**, *324*, 1530–1534.
3. Bae, S.; Kim, H.; Lee, Y.; Xu, X.; Park, J.-S.; Zheng, Y.; Balakrishnan, J.; Lei, T.; Ri Kim, H.; Song, Y. I.; *et al.* Roll-to-Roll Production of 30-in. Graphene Films for Transparent Electrodes. *Nat. Nano.* **2010**, *5*, 574–578.
4. Loh, K. P.; Bao, Q.; Ang, P. K.; Yang, J. The Chemistry of Graphene. *J. Mater. Chem.* **2010**, 20.
5. Zhan, D.; Yan, J.; Lai, L.; Ni, Z.; Liu, L.; Shen, Z. Engineering the Electronic Structure of Graphene. *Adv. Mater.* **2012**, *24*, 4055–4069.
6. Guinea, F.; Katsnelson, M. I.; Geim, A. K. Energy Gaps and a Zero-Field Quantum Hall effect in Graphene by Strain Engineering. *Nat. Phys.* **2010**, *6*, 30–33.
7. Yeh, N. C.; Teague, M. L.; Yeom, S.; Standley, B. L.; Wu, R. T. P.; Boyd, D. A.; Bockrath, M. W. Strain-Induced Pseudomagnetic Fields and Charging Effects on CVD-grown Graphene. *Surf. Sci.* **2011**, *605*, 1649–1656.
8. Huang, M.; Yan, H.; Heinz, T. F.; Hone, J. Probing Strain-Induced Electronic Structure Change in Graphene by Raman Spectroscopy. *Nano Lett.* **2010**, *10*, 4074–4079.
9. Gong, L.; Kinloch, I. A.; Young, R. J.; Riaz, I.; Jalil, R.; Novoselov, K. S. Interfacial Stress Transfer in a Graphene Monolayer Nanocomposite. *Adv. Mater.* **2010**, *22*, 2694–2697.
10. Srivastava, I.; Mehta, R. J.; Yu, Z.-Z.; Schadler, L.; Koratkar, N. Raman Study of Interfacial Load Transfer in Graphene Nanocomposites. *Appl. Phys. Lett.* **2011**, *98*, 063102–3.
11. Gong, L.; Young, R. J.; Kinloch, I. A.; Riaz, I.; Jalil, R.; Novoselov, K. S. Optimizing the Reinforcement of Polymer-Based Nanocomposites by Graphene. *ACS Nano* **2012**, *6*, 2086–2095.
12. He, R.; Zhao, L.; Petrone, N.; Kim, K. S.; Roth, M.; Hone, J.; Kim, P.; Pasupathy, A.; Pinczuk, A. Large Physisorption Strain in Chemical Vapor Deposition of Graphene on Copper Substrates. *Nano Lett.* **2012**, *12*, 2408–2413.
13. Wang, Y. Y.; Ni, Z. H.; Yu, T.; Shen, Z. X.; Wang, H. M.; Wu, Y. H.; Chen, W.; Shen Wee, A. T. Raman Studies of Monolayer Graphene: The Substrate Effect. *J. Phys. Chem. C* **2008**, *112*, 10637–10640.
14. Kim, K. S.; Zhao, Y.; Jang, H.; Lee, S. Y.; Kim, J. M.; Kim, K. S.; Ahn, J.-H.; Kim, P.; Choi, J.-Y.; Hong, B. H. Large-Scale Pattern Growth of Graphene Films for Stretchable Transparent Electrodes. *Nature* **2009**, *457*, 706–710.
15. Lee, S.-K.; Kim, B. J.; Jang, H.; Yoon, S. C.; Lee, C.; Hong, B. H.; Rogers, J. A.; Cho, J. H.; Ahn, J.-H. Stretchable Graphene Transistors with Printed Dielectrics and Gate Electrodes. *Nano Lett.* **2011**, *11*, 4642–4646.
16. Fu, X.-W.; Liao, Z.-M.; Zhou, J.-X.; Zhou, Y.-B.; Wu, H.-C.; Zhang, R.; Jing, G.; Xu, J.; Wu, X.; Guo, W.; *et al.* Strain Dependent Resistance in Chemical Vapor Deposition Grown Graphene. *Appl. Phys. Lett.* **2011**, *99*, 213107.
17. Ni, Z. H.; Wang, H. M.; Ma, Y.; Kasim, J.; Wu, Y. H.; Shen, Z. X. Tunable Stress and Controlled Thickness Modification in Graphene by Annealing. *ACS Nano* **2008**, *2*, 1033–1039.
18. Ni, Z. H.; Yu, T.; Lu, Y. H.; Wang, Y. Y.; Feng, Y. P.; Shen, Z. X. Uniaxial Strain on Graphene: Raman Spectroscopy Study and Band-Gap Opening. *ACS Nano* **2008**, *2*, 2301–2305.
19. Yu, T.; Ni, Z.; Du, C.; You, Y.; Wang, Y.; Shen, Z. Raman Mapping Investigation of Graphene on Transparent Flexible Substrate: The Strain Effect. *J. Phys. Chem. C* **2008**, *112*, 12602–12605.
20. Huang, M.; Yan, H.; Chen, C.; Song, D.; Heinz, T. F.; Hone, J. Phonon Softening and Crystallographic Orientation of Strained Graphene Studied by Raman Spectroscopy. *Proc. Natl. Acad. Sci. U.S.A.* **2009**, *106*, 7304–7308.
21. Metzger, C.; Rémi, S.; Liu, M.; Kusminskiy, S. V.; Castro Neto, A. H.; Swan, A. K.; Goldberg, B. B. Biaxial Strain in Graphene Adhered to Shallow Depressions. *Nano Lett.* **2009**, *10*, 6–10.
22. Tsoukleri, G.; Parthenios, J.; Papagelis, K.; Jalil, R.; Ferrari, A. C.; Geim, A. K.; Novoselov, K. S.; Galiotis, C. Subjecting a Graphene Monolayer to Tension and Compression. *Small* **2009**, *5*, 2397–2402.
23. Choi, S.-M.; Jhi, S.-H.; Son, Y.-W. Effects of Strain on Electronic Properties of Graphene. *Phys. Rev. B* **2010**, *81*, 081407.
24. Ding, F.; Ji, H.; Chen, Y.; Herklotz, A.; Dörr, K.; Mei, Y.; Rastelli, A.; Schmidt, O. G. Stretchable Graphene: A Close Look at Fundamental Parameters through Biaxial Straining. *Nano Lett.* **2010**, *10*, 3453–3458.
25. Frank, O.; Tsoukleri, G.; Parthenios, J.; Papagelis, K.; Riaz, I.; Jalil, R.; Novoselov, K. S.; Galiotis, C. Compression Behavior of Single-Layer Graphenes. *ACS Nano* **2010**, *4*, 3131–3138.
26. Yin, Z.; Sun, S.; Salim, T.; Wu, S.; Huang, X.; He, Q.; Lam, Y. M.; Zhang, H. Organic Photovoltaic Devices Using Highly Flexible Reduced Graphene Oxide Films as Transparent Electrodes. *ACS Nano* **2010**, *4*, 5263–5268.
27. Frank, O.; Mohr, M.; Maultzsch, J.; Thomsen, C.; Riaz, I.; Jalil, R.; Novoselov, K. S.; Tsoukleri, G.; Parthenios, J.; Papagelis, K.; *et al.* Raman 2D-Band Splitting in Graphene: Theory and Experiment. *ACS Nano* **2011**, *5*, 2231–2239.
28. Frank, O.; Tsoukleri, G.; Riaz, I.; Papagelis, K.; Parthenios, J.; Ferrari, A. C.; Geim, A. K.; Novoselov, K. S.; Galiotis, C. Development of a Universal Stress Sensor for Graphene and Carbon Fibres. *Nat. Commun.* **2011**, *2*, 255.
29. Wang, Y.; Yang, R.; Shi, Z.; Zhang, L.; Shi, D.; Wang, E.; Zhang, G. Super-elastic Graphene Ripples for Flexible Strain Sensors. *ACS Nano* **2011**, *5*, 3645–3650.
30. Yoon, D.; Son, Y.-W.; Cheong, H. Strain-Dependent Splitting of the Double-Resonance Raman Scattering Band in Graphene. *Phys. Rev. Lett.* **2011**, *106*, 155502.
31. Young, R. J.; Gong, L.; Kinloch, I. A.; Riaz, I.; Jalil, R.; Novoselov, K. S. Strain Mapping in a Graphene Monolayer Nanocomposite. *ACS Nano* **2011**, *5*, 3079–3084.
32. Zabel, J.; Nair, R. R.; Ott, A.; Georgiou, T.; Geim, A. K.; Novoselov, K. S.; Casiraghi, C. Raman Spectroscopy of Graphene and Bilayer under Biaxial Strain: Bubbles and Balloons. *Nano Lett.* **2011**, *12*, 617–621.
33. Mohiuddin, T. M. G.; Lombardo, A.; Nair, R. R.; Bonetti, A.; Savini, G.; Jalil, R.; Bonini, N.; Basko, D. M.; Galiotis, C.; Marzari, N.; *et al.* Uniaxial Strain in Graphene by Raman Spectroscopy: G Peak Splitting, Grüneisen Parameters, and Sample Orientation. *Phys. Rev. B* **2009**, *79*, 205433.
34. Ago, H.; Ogawa, Y.; Tsuji, M.; Mizuno, S.; Hibino, H. Catalytic Growth of Graphene: Toward Large-Area Single-Crystalline Graphene. *J. Phys. Chem. Lett.* **2012**, *3*, 2228–2236.
35. Wood, J. D.; Schmucker, S. W.; Lyons, A. S.; Pop, E.; Lyding, J. W. Effects of Polycrystalline Cu Substrate on Graphene Growth by Chemical Vapor Deposition. *Nano Lett.* **2011**, *11*, 4547–4554.
36. Huang, P. Y.; Ruiz-Vargas, C. S.; van der Zande, A. M.; Whitney, W. S.; Levendorf, M. P.; Kevek, J. W.; Garg, S.; Alden, J. S.; Hustedt, C. J.; Zhu, Y.; *et al.* Grains and Grain Boundaries in Single-Layer Graphene Atomic Patchwork Quilts. *Nature* **2011**, *469*, 389–392.
37. Kim, K.; Lee, Z.; Regan, W.; Kisielowski, C.; Crommie, M. F.; Zettl, A. Grain Boundary Mapping in Polycrystalline Graphene. *ACS Nano* **2011**, *5*, 2142–2146.
38. Yazyev, O. V.; Louie, S. G. Electronic Transport in Polycrystalline Graphene. *Nat. Mater.* **2010**, *9*, 806–809.

39. Ogawa, Y.; Hu, B.; Orofeo, C. M.; Tsuji, M.; Ikeda, K.-i.; Mizuno, S.; Hibino, H.; Ago, H. Domain Structure and Boundary in Single-Layer Graphene Grown on Cu(111) and Cu(100) Films. *J. Phys. Chem. Lett.* **2011**, *3*, 219–226.
40. Orofeo, C. M.; Hibino, H.; Kawahara, K.; Ogawa, Y.; Tsuji, M.; Ikeda, K.-i.; Mizuno, S.; Ago, H. Influence of Cu Metal on the Domain Structure and Carrier Mobility in Single-Layer Graphene. *Carbon* **2012**, *50*, 2189–2196.
41. Kim, J.; Lee, C.; Bae, S.; Kim, S. J.; Kim, K. S.; Hong, B. H.; Choi, E. J. Effect of Uni-Axial Strain on THz/Far-Infrared Response of Graphene. *Appl. Phys. Lett.* **2012**, *100*, 041910–4.
42. Suk, J. W.; Kitt, A.; Magnuson, C. W.; Hao, Y.; Ahmed, S.; An, J.; Swan, A. K.; Goldberg, B. B.; Ruoff, R. S. Transfer of CVD-Grown Monolayer Graphene onto Arbitrary Substrates. *ACS Nano* **2011**, *5*, 6916–6924.
43. Song, H. S.; Li, S. L.; Miyazaki, H.; Sato, S.; Hayashi, K.; Yamada, A.; Yokoyama, N.; Tsukagoshi, K. Origin of the Relatively Low Transport Mobility of Graphene Grown through Chemical Vapor Deposition. *Sci. Rep.* **2012**, *2*, 1–6.
44. Li, X.; Cai, W.; An, J.; Kim, S.; Nah, J.; Yang, D.; Piner, R.; Velamakanni, A.; Jung, I.; Tutuc, E.; *et al.* Large-Area Synthesis of High-Quality and Uniform Graphene Films on Copper Foils. *Science* **2009**, *324*, 1312–1314.
45. Castro, E. V.; Ochoa, H.; Katsnelson, M. I.; Gorbachev, R. V.; Elias, D. C.; Novoselov, K. S.; Geim, A. K.; Guinea, F. Limits on Charge Carrier Mobility in Suspended Graphene Due to Flexural Phonons. *Phys. Rev. Lett.* **2010**, *105*, 266601.
46. Xu, Y. N.; Zhan, D.; Liu, L.; Suo, H.; Ni, Z. H.; Nguyen, T. T.; Zhao, C.; Shen, Z. X. Thermal Dynamics of Graphene Edges Investigated by Polarized Raman Spectroscopy. *ACS Nano* **2010**, *5*, 147–152.
47. Kotakoski, J.; Meyer, J. C. Mechanical Properties of Polycrystalline Graphene Based on a Realistic Atomistic Model. *Phys. Rev. B* **2012**, *85*, 195447.
48. Grantab, R.; Shenoy, V. B.; Ruoff, R. S. Anomalous Strength Characteristics of Tilt Grain Boundaries in Graphene. *Science* **2010**, *330*, 946–948.
49. Hao, F.; Fang, D. Mechanical Deformation and Fracture Mode of Polycrystalline Graphene: Atomistic Simulations. *Phys. Lett. A* **2012**, *376*, 1942–1947.
50. Qi, Z.; Park, H. S. Intrinsic Energy Dissipation in CVD-Grown Graphene Nanoresonators. *Nanoscale* **2012**, *4*, 3460–3465.
51. Zhang, Y.; Gao, T.; Gao, Y.; Xie, S.; Ji, Q.; Yan, K.; Peng, H.; Liu, Z. Defect-like Structures of Graphene on Copper Foils for Strain Relief Investigated by High-Resolution Scanning Tunneling Microscopy. *ACS Nano* **2011**, *5*, 4014–4022.
52. Malard, L. M.; Pimenta, M. A.; Dresselhaus, G.; Dresselhaus, M. S. Raman Spectroscopy in Graphene. *Phys. Rep.* **2009**, *473*, 51–87.
53. Dresselhaus, M. S.; Jorio, A.; Hofmann, M.; Dresselhaus, G.; Saito, R. Perspectives on Carbon Nanotubes and Graphene Raman Spectroscopy. *Nano Lett.* **2010**, *10*, 751–758.
54. Dresselhaus, M. S.; Jorio, A.; Saito, R. Characterizing Graphene, Graphite, and Carbon Nanotubes by Raman Spectroscopy. *Annu. Rev. Condens. Mater. Phys.* **2010**, *1*, 89–108.
55. Cheng, Y. C.; Zhu, Z. Y.; Huang, G. S.; Schwingenschlögl, U. Grüneisen Parameter of the G Mode of Strained Monolayer Graphene. *Phys. Rev. B* **2011**, *83*, 115449.
56. Geng, D.; Wu, B.; Guo, Y.; Huang, L.; Xue, Y.; Chen, J.; Yu, G.; Jiang, L.; Hu, W.; Liu, Y. Uniform Hexagonal Graphene Flakes and Films Grown on Liquid Copper Surface. *Proc. Natl. Acad. Sci. U.S.A.* **2012**, 10.1073/pnas.1200339109.
57. Robertson, A. W.; Warner, J. H. Hexagonal Single Crystal Domains of Few-Layer Graphene on Copper Foils. *Nano Lett.* **2011**, *11*, 1182–1189.
58. Chandra, N.; Namilae, S.; Shet, C. Local Elastic Properties of Carbon Nanotubes in the Presence of Stone-Wales Defects. *Phys. Rev. B* **2004**, *69*, 094101.
59. Banhart, F.; Kotakoski, J.; Krasheninnikov, A. V. Structural Defects in Graphene. *ACS Nano* **2010**, *5*, 26–41.
60. Terrones, H.; Lv, R.; Terrones, M.; Dresselhaus, M. S. The Role of Defects and Doping in 2D Graphene Sheets and 1D Nanoribbons. *Rep. Prog. Phys.* **2012**, *75*, 062501.
61. Kudin, K. N.; Ozbas, B.; Schniepp, H. C.; Prud'homme, R. K.; Aksay, I. A.; Car, R. Raman Spectra of Graphite Oxide and Functionalized Graphene Sheets. *Nano Lett.* **2007**, *8*, 36–41.
62. Semenoff, G. W.; Semenoff, V.; Zhou, F. Domain Walls in Gapped Graphene. *Phys. Rev. Lett.* **2008**, *101*, 087204.
63. Lahiri, J.; Lin, Y.; Bozkurt, P.; Oleynik, I. I.; Batzill, M. An Extended Defect in Graphene as a Metallic Wire. *Nat. Nanotechnol.* **2010**, *5*, 326–329.
64. Reich, S.; Jantoljak, H.; Thomsen, C. Shear Strain in Carbon Nanotubes Under Hydrostatic Pressure. *Phys. Rev. B* **2000**, *61*, R13389–R13392.
65. Khang, D.-Y.; Jiang, H.; Huang, Y.; Rogers, J. A. A Stretchable Form of Single-Crystal Silicon for High-Performance Electronics on Rubber Substrates. *Science* **2006**, *311*, 208–212.
66. Mohr, M.; Papagelis, K.; Maultzsch, J.; Thomsen, C. Two-Dimensional Electronic and Vibrational Band Structure of Uniaxially Strained Graphene from *ab Initio* Calculations. *Phys. Rev. B* **2009**, *80*, 205410.
67. Novoselov, K. S.; Geim, A. K.; Morozov, S. V.; Jiang, D.; Zhang, Y.; Dubonos, S. V.; Grigorieva, I. V.; Firsov, A. A. Electric Field Effect in Atomically Thin Carbon Films. *Science* **2004**, *306*, 666–669.